

Document downloaded from:

<http://hdl.handle.net/10251/107414>

This paper must be cited as:

Doménech Carbó, A.; Domenech Carbo, MT.; Álvarez-Romero, C.; Montoya, N.; Pasies-Oviedo, T.; Buendía Ortuño, MDM. (2017). Electrochemical Characterization of Coinage Techniques the 17(th) Century: The maravedis Case. *Electroanalysis*. 29(9):2008-2018. doi:10.1002/elan.201700326



The final publication is available at

<http://doi.org/10.1002/elan.201700326>

Copyright John Wiley & Sons

Additional Information

Electrochemical characterization of coinage techniques the 17th century: The *maravedís* case

Antonio Doménech-Carbó^{*a}, María Teresa Doménech-Carbó^b, Carla Álvarez^b, Noemí Montoya^a, Trinidad Pasíes^c, Milagros Buendía^d

^a Departament de Química Analítica. Universitat de València. Dr. Moliner, 50, 46100 Burjassot (València) Spain.

^b Institut de Restauració del Patrimoni, Universitat Politècnica de València, Camí de Vera 14, 46022, València, Spain.

^c Museu de Prehistòria de València. Corona 36, 46003, Valencia, Spain.

^d Museo nacional de Arqueología Subacuática, Cartagena, Spain.

* Corresponding author; e-mail: antonio.domenech@uv.es

Abstract

The voltammetry of immobilized particles (VIMP) methodology was applied to the discrimination of Spanish *maravedís* produced in 10 different mints between 1661 and 1664 using characteristic signatures for the reduction of cuprite and tenorite in the patina of the coins and catalytic effects on the hydrogen evolution reaction (HER). The variation of the apparent tenorite/cuprite ratio with depth was fitted to potential laws differing from one mint to another for A Coruña, Burgos, Córdoba, Cuenca, Granada, Madrid, Trujillo, Segovia, Sevilla and Valladolid coins. Electrochemical data permitted to detect the changes in the composition (with lowering of the silver content) and manufacturing technique (from hammer to mill) occurring in this historical period.

Keywords: Electrochemistry; Archaeometry; Mint discrimination; Coins; Corrosion products.

Introduction

Coins constitute an important source of information of historical and archaeological value. Determining the provenance of raw materials, characterizing the fabrication technique and discriminating between different series of coins and/or mints are in general required for archaeometric studies. This information can be derived from the elucidation of coin composition and metallographic structure [1,2] and other spectroscopic and diffraction techniques [3-8] including isotope analysis [9,10]. Acquiring this information, however, requires more or less invasive sampling within the metal core, which is only allowed for archaeological objects under very specific conditions [11,12]. By this reason, there is an obvious interest in analytical techniques aimed to acquire archaeometric information from the examination of the metal patina [13-16].

Among these techniques, the voltammetry of immobilized particles (VIMP), a solid-state electrochemical methodology developed by Scholz et al. [17,18], appears as a potentially interesting because of its inherently high sensitivity and its requirement of amounts of sample at the sub-microgram level [19,20]. This technique has been applied to the identification of metals and their corrosion products [21-27]. The use of minimally invasive sampling strategies [28,29] permitted its use for mapping [30] and layer-by-layer analysis [31] of metal patinas as well as for authentication [32,33] and dating [34,35] of archaeological metal.

In this context, we have previously reported applications of VIMP for screening different series of copper-based coins [36-39] supporting the idea that light differences in the composition and metallography of the coins are reflected in the voltammetric response of the corrosion patina. Here, we extend this approach: i) considering the presence of silver in the coin composition, and ii) using voltammetric data for the hydrogen evolution reaction (HER), providing a theoretical model for describing the electrochemical discrimination of different mints based on modeling the depth variation of the composition of the corrosion layers of the coins. The VIMP study, complemented by Raman spectroscopy and ion beam-field emission scanning electron microscopy (FIB-FESEM), was applied to the discrimination of monetary series of Spanish *maravedis*.

During the 16th and 17th centuries counterfeiting of coins was one of the greatest problems suffered by the Kingdoms [40,41]. On October 29, 1660, Felipe IV, the **Spain** King, ordered to coin a new series of fleece by Pragmatic in El Escorial. After almost sixty years (from 1602) of coinage of pure copper, the silver alloy was introduced again [40,42]. In addition, in this Pragmatic, the type that should appear in each *maravedí* was perfectly defined depending on its value: on the obverse would be the bust of the king, while on the anverse, for the value of two *maravedís* would appear a lion, in the one of four a castle, in the one of eight a shield with two castles and two lions, and in the sixteenth the complete coat of arms of the royal house [40,42].

However, the difficulty of maintaining the silver value and other technical aspects motivated that this series of coins, which were initially minted by mill, began to mince by hammer as early as 1661. But that same year, the type of hammer coinage was banned by a October 30 proclamation at the same time as its circulation [40-43]. These pieces were minted in most of the mints of the kingdom in great abundance, until, on October 14, 1664, a new Pragmatic reduced its value in half [42,43] and the coinage of this type of coins ceased.

The study of these coins is particularly interesting because along the 17th century, the fiscal and monetary policies adopted by the Spanish crown were strongly conditioned by its ambitious foreign policy and the dependence on the arrival of American silver [44,45] resulting in important inflationary pressure which motivated a series of documented debasements by means of issues of petty copper coins or increasing its **nominal** value (*resellos*) [46-48]. The obtained electrochemical data, based on a set of *maravedís* produced between 1661 and 1664 in 10 different mints permitted to draw a picture descriptive of the successive modifications introduced in the currency.

2. Experimental

2.1. Samples

A set of 40 *maravedís* coins (M01 to M40 in the following) from the Prehistory Museum of Valencia were studied. These include 38 coins from 10 different mints (A Coruña, Burgos, Córdoba, Cuenca, Granada, Madrid, Segovia, Sevilla, Trujillo and Valladolid) and two coins whose numismatic characteristics permitted their consideration as falsifications. The studied coins were selected as those produced between 1661 and 1664 allowing to identify the year of emission, the mark identifying the mint and presenting an uniform, moderate corrosion as judged by the uniformity of the brownish hue (see Figure 1) and the absence of localized aggregates of green corrosion products. Sampling was performed with commercial paraffin-impregnated graphite bars (Alpino, HB type, 2.0 mm diameter) by pressing and lightly rotating it onto a smooth region of the coin surface during ca. 5 s. One, two or three samples were taken for each coin depending on the availability of regions of uniformly colored plane surface. To avoid 'memory' effects, numbering of samples and voltammetric measurements were performed after randomized distribution of the coins.

2.2. Instrumentation and methods

Electrochemical experiments were performed at 298 K in a three-electrode cell using a CH I660C device (Cambria Scientific, Llwynhendy, Llanelli UK). Air-saturated aqueous 0.25 M sodium acetate buffer (Panreac) at pH 4.50 was used as a supporting electrolyte for electrochemical measurements and was renewed after each electrochemical run to avoid contamination due to metal ions eventually released to the solution phase during electrochemical turnovers. To test the possibility of using portable equipment, no deaeration was performed. Square wave voltammograms (SWVs), and cyclic voltammograms (CVs) were obtained on sample-modified graphite electrodes, a platinum wire counterelectrode and an Ag/AgCl (3 M NaCl) reference electrode completing the three-electrode arrangement.

VIMP for reference materials was carried out using conventional VIMP protocols by powdering an amount of 1-2 mg of the solid in an agate mortar and pestle, and extending it on the agate mortar forming a spot of finely distributed material. Then the lower end of the graphite electrode was gently rubbed over that spot of sample and finally rinsed with water to remove ill-adhered particles. Sample-modified graphite bars

were then dipped into the electrochemical cell so that only the lower end of the electrode was in contact with the electrolyte solution.

Raman spectra of different coins were obtained by means of a XPlora Horiba MTB model and a 532 nm laser as excitation with maximum power of 90 mW. The samples were measured in backscattering geometry at room temperature. A 100 confocal microscope objective was used to focus the excitation laser on the sample and collect the scattered light to the spectrometer. More than 3 different areas were analyzed per sample, to obtain representative results. Exposure time, number of acquisitions and laser power varied among 5 – 20 s, 10 – 50 and 30 – 80 mW, respectively. Data acquisition was carried out with the LabSpec 6 Spectroscopy Suite from Horiba MTB.

The microstructure of coins was determined using field emission scanning electron microscopy (Model S-4800, Hitachi Ltd., Tokyo, Japan) operating at 20 kV. The microanalysis of samples was performed with X-ray microanalysis system (SEM/EDX). Photographic images of coins were carried out with a Leica M165 stereo microscope using a capture system of high resolution digital image IC80HD controlled by LAS program. Sectioning and imaging of the coins was performed with a FIB-FESEM Zeiss (Orsay Physics Kleindiek Oxford Instruments) model Auriga compact equipment that enabled the characterization of the microtexture and mineral phases in the superficial corrosion layer and in the metal core of the 19th century coins. The operating conditions were: voltage, 30 kV and current intensity, 500 μ A and 20 nA in the FIB for generating the focused beam of Ga ions and a voltage of 3 kV in the FESEM.

3. Results and discussion

3.1. Organoleptic properties and corrosion products

The studied coins were selected as exhibiting a moderate state of corrosion, with an uniform brownish hue. Figure 1 shows the Raman spectrum of coin **M30**, accompanied by a photographic image of that coin, in which the main cuprite bands at 103, 151, 218, 420 and 630 cm^{-1} and the principal tenorite bands at 290, 337 and 620 cm^{-1} appear [49,50].

SEM/EDX was performed to obtain information on the surface distribution of silver and copper. The elemental composition determined by EDX is shown in Figure 2 for two different coins a) M22 and b) M01. It could be observed the variation of silver and copper with the coins, in the mint M22 is just found compounds of copper on the surface whereas in the coin M01 silver compounds appeared with the copper compounds. These results were contrasted performing microanalysis by mapping when the main compounds, silver and copper, are selected. It can be noted that for the coin M22 (Fig. 2c)) copper is found in greater quantity of copper compounds all over the surface and in the case of the coin M01 (Fig. 2d)) is presented silver compound in low quantity in localized areas with copper as a major compound in all area.

3.2. Voltammetric pattern

Figure 3 depicts a series of replicate square wave voltammograms of samples from coins a,b) M35, c,d) M31 and d,e) M26 attached to graphite electrodes immersed into air-saturated 0.25 M HAc/NaAc at pH 4.50. Such coins, all minted in Madrid, are representative of the three electrochemical types (I, II and III, respectively, *vide infra*) in which the production of this mint can be divided. In negative-going voltammograms (Fig. 3a,c), a main cathodic peak appears at -0.10 V vs. Ag/AgCl (C_1) which is followed by more or less well-defined shoulders at -0.30 (C_2) and -0.70 V (C_{ox}), preceding the rising current for the hydrogen evolution reaction (HER). In positive-going voltammograms (Fig. 3b,d) a main tall oxidation peak appears at 0.0 V (A_1), usually presenting peak splitting, often followed by a second oxidation peak at $+0.45$ V (A_{Ag}). This voltammetry can be interpreted on the basis of abundant literature on copper [24-26] and silver [36,37,51,52] corrosion products and previous results [27,31]. Accordingly, the peak C_1 can be attributed to the reduction of cuprite (Cu_2O) superimposed to the reduction of copper corrosion products of the malachite, brochantite and/or atacamite minerals, often accompanied by the reduction of AgCl. The signal C_2 corresponds to the reduction of tenorite (CuO) whereas the signal C_{ox} can be attributed to the reduction of dissolved oxygen, a well-known electrochemical process [53,54]. The signals recorded in positive-going potential scans can be unambiguously attributed to the oxidative dissolution of the metal deposits generated as a result of the above reduction processes. The peak A_1 corresponds to copper oxidation and the peak A_2 to the oxidation of silver to silver acetate [36,37,51,52].

Given the abrasive nature of the sampling process, variable amounts of corrosion products were transferred to the electrode surface so that, as can be seen in **Figure 3**, replicate experiments on the same coin produced differences in the peak height. For our purposes, two relevant points have to be emphasized: i) for each coin, the ratio between the current at the shoulder C_2 and the peak C_1 , $i(C_2)/i(C_1)$, decreased monotonically on increasing the absolute value of the current $i(C_1)$ in replicate experiments such as in **Figure 3**; ii) the data for different coins were grouped along different curved paths, as illustrated in **Figure 4** for *maravedis* produced in the Madrid mint in years 1661 – 1664. One can see in this figure that a significant portion of the coins **minted** in 1661 were grouped around one curve (Madrid-I) whereas other 1661 *maravedis* and those produced in 1662 were grouped into a second, clearly separated curve (Madrid-II) and, finally, the studied *maravedis* coined in 1663 and 1664 were grouped around a third curved of tendency (Madrid-III). **Representative voltammograms of each one of these voltammetric types were depicted in Figure 3 and Figures S1 to S4 in Supplementary information.** These results suggested that the tenorite/cuprite ratio, in principle expressed by the $i(C_2)/i(C_1)$ ratio, decreased on increasing the amount of sample transferred to the **graphite** electrode from the corrosion layers, represented by the absolute value of these peak currents. This feature can be interpreted on assuming that there is a concentration gradient of copper oxides in the corrosion layers, as treated in detail below.

3.3. FESEM-FIB data

The appearance of different types of voltammetric response and sample grouping as depicted in **Figure 4** suggested that, for coins with a similar ‘corrosion history’, the voltammetry of the corrosion layers depends on the chemical composition of the base alloy and its metallographic properties derived from the thermomechanical treatment carried out during the coin manufacturing. Both aspects can be studied from FIB-FESEM-EDX experiments where a Ga ions microbeam perforates trenches of *ca.* 10 μm length and *ca.* 15 μm depth. These trenches are not detectable at the macroscopic level and provide sections of the metal core and corrosion layers. **Figure 5** presents the secondary electron images and elemental depth profiles of coins M19 and M22 recorded in trenches of *ca.* 10 μm length and *ca.* 15 μm depth generated by the ionic beam.

In the case of coin M09, **minted in Madrid in 1661**, representative of the Madrid-I voltammetric type, the corrosion layer appears as undifferentiated from the metal core, although exhibiting irregular crevices. The metallic region consists of 1-2 μm -sized domains intercalated into an apparently continuous matrix. The proportion of silver relative to copper was enhanced in different regions and in the more external layer of the coin. In contrast, coin M22, **minted in Madrid in 1664 and** representative of the Madrid-III electrochemical type, presented a segregated corrosion layer while the metal core consisted of different crystalline domains between 1 and 8 μm . No silver was detected by the EDX system in this case.

The above data indicate that there are relevant differences in the texture of the corrosion layer in the upper region of the trench and in microtexture of the metal as well as in the composition and depth distribution of copper and silver, in agreement with previous data on mediaeval [37] and modern [39] coins.

3.4. Modeling depth variation of voltammetric and compositional parameters

Under our experimental conditions, VIMP measurements involve the transference of nanogram amounts of the corrosion layers to the graphite bar which is pressed on the coin surface. Then, if the pressure is low, sampling removes small amounts of corrosion products and their composition will be representative of the external regions. When the sampling pressure was larger, the amount of sample increased and its composition will be representative of upper and lower regions of the corrosion layers. Now, let us assume that a graphite bar of section S_0 was pressed onto the coin surface so that a net volume V of corrosion products was transferred to the electrode surface during the sampling process. If the sampled depth z was clearly lower than the diameter of the graphite bar, the sampled volume will be proportional to the reached depth so that $dV = Sdz$, $S \ll S_0$ being the surface of the graphite bar covered by the microparticulate sample

Copper-silver alloys are present as either non-equilibrium solid solutions or two-phase microstructures [53]. In silver-copper solid solutions there is possibility of internal oxidation with copper corroding preferentially to form copper compounds [54,55]. Silver oxidation species (chloride, sulfide, or oxide, mainly) can also be formed; the

nature of the corrosion product is therefore highly dependent upon the corrosion environment [56]. Now, let us assume that corrosion proceeds via formation of local cells yielding a primary patina of cuprite and AgCl subsequently growing and forming a more permeable secondary patina, as described by Robbiola et al. for copper/bronze objects [15]. It will be assumed that the growth of Cu₂O and AgCl occurs independently and at different rates. Taken into account that the secondary patina is progressively enriched in tenorite, whose formation through the aerobic oxidation of cuprite is thermodynamically spontaneous [57,58], the number of tenorite grains per volume unit, n_{ten} , will increase from zero in the primary/secondary patina boundary ($z = \delta$) to a value $n_{\text{ten}}^{\text{sup}}$ at the external surface of the secondary patina ($z = 0$). Concomitantly, the number of cuprite and AgCl grains per volume unit, n_{cup} , n_{AgCl} , respectively, will decrease from their values in the primary patina, $n_{\text{cup}}^{\text{o}}$, $n_{\text{AgCl}}^{\text{o}}$, to surface values of $n_{\text{cup}}^{\text{sup}}$, $n_{\text{AgCl}}^{\text{sup}}$.

This situation can be approximated upon assuming that different concentration gradients exist for cuprite/tenorite and AgCl. Then, considering that in VIMP experiments one obtains separate signals for the reduction of cuprite plus AgCl (C_1) and tenorite (C_2) grains, one can write (in the absence of other interfering components):

$$i(C_1) = \int_0^z \varepsilon_{\text{cup}} S [n_{\text{cup}}^{\text{o}} - n_{\text{ten}}^{\text{sup}} f(z)] dz + \int_0^z \varepsilon_{\text{AgCl}} S [n_{\text{AgCl}}^{\text{o}} - n_{\text{AgCl}}^{\text{sup}} g(z)] dz \quad (1)$$

$$i(C_2) = \int_0^V \varepsilon_{\text{ten}} n_{\text{ten}} dV = \int_0^y \varepsilon_{\text{ten}} n_{\text{ten}}^{\text{sup}} S f(z) dz \quad (2)$$

In these equations, $f(z)$ and $g(z)$ represent the gradient functions for cuprite/tenorite and AgCl, and ε_{cup} , ε_{ten} , $\varepsilon_{\text{AgCl}}$, electrochemical constants characterizing the respective reduction processes. Such constants will be dependent on the electrochemical conditions, i.e., electrolyte, temperature, potential scan rate, etc. In agreement with previous data on copper coins,³⁸ the best fit of experimental data was obtained for potential gradients of the form $f(z) = z^\alpha$, and $g(z) = z^\beta$. Then, integration of the above equations yields:

$$i(C_2) = \frac{\varepsilon_{\text{ten}} S n_{\text{ten}}^{\text{sup}}}{1 + \alpha} z^{1+\alpha} \quad (3)$$

$$i(C_1) = \frac{\varepsilon_{\text{cup}} S}{1 + \alpha} \left[(1 + \alpha) n_{\text{cup}}^{\circ} z - n_{\text{ten}}^{\text{sup}} z^{1+\alpha} \right] + \frac{\varepsilon_{\text{AgCl}} S}{1 + \beta} \left[(1 + \beta) n_{\text{AgCl}}^{\circ} z - n_{\text{AgCl}}^{\text{sup}} z^{1+\beta} \right] \quad (4)$$

If the conversion of cuprite into tenorite was not extensive, a reasonable assumption under ordinary conditions, one can approximate:

$$i(C_1) \approx zS(\varepsilon_{\text{cup}} n_{\text{cup}}^{\circ} + \varepsilon_{\text{AgCl}} n_{\text{AgCl}}^{\circ}) \quad (5)$$

Then, taking $\alpha \approx \beta$, the peak current ratio can be expressed as a function of $i(C_1)$:

$$\frac{i(C_2)}{i(C_1)} = \frac{\varepsilon_{\text{ten}} n_{\text{ten}}^{\text{sup}} i(C_1)^{\alpha} / S^{\alpha} (\varepsilon_{\text{cup}} n_{\text{cup}}^{\circ} + \varepsilon_{\text{AgCl}} n_{\text{AgCl}}^{\circ})^{\alpha}}{(1 + \alpha) \varepsilon_{\text{cup}} n_{\text{cup}}^{\circ} + (1 + \beta) \varepsilon_{\text{AgCl}} n_{\text{AgCl}}^{\circ} - \frac{\left(\varepsilon_{\text{cup}} n_{\text{ten}}^{\text{sup}} + \frac{1 + \beta}{1 + \alpha} \varepsilon_{\text{AgCl}} n_{\text{AgCl}}^{\text{sup}} \right)}{S^{\alpha} (\varepsilon_{\text{cup}} n_{\text{cup}}^{\circ} + \varepsilon_{\text{AgCl}} n_{\text{AgCl}}^{\circ})^{\alpha}} i(C_1)^{\alpha}} \quad (6)$$

Equation (6) predicts a relationship between the $i(C_2)/i(C_1)$ ratio and $i(C_1)$ which can be approximated to a potential law of the form:

$$\frac{i(C_2)}{i(C_1)} = \frac{Ai(C_1)^{\alpha}}{B + i(C_1)^{\alpha}} \approx \frac{A}{B} i(C_1)^{\alpha} \quad (7)$$

where both A and B terms depend on the composition of the corrosion products of copper and silver in the extremes of the secondary patina. In the absence of silver, Eq. (7) reduces to that previously reported for copper coins [38]. Since ε_{ten} , ε_{cup} and S will be the same for each series of coins, the differences in the parameters $n_{\text{ten}}^{\text{sup}}$, n_{cup}° , α , b , will be dependent on the characteristics of the corrosion layer, in turn depending on the composition of the base alloy, its metallographic structure and the conditions of corrosion. Accordingly, the $i(C_2)/i(C_1)$ vs. $i(C_1)$ plots should be different for samples from different monetary emissions submitted to a similar corrosion process.

In the positive-going potential scans, one obtains the stripping peaks corresponding to the oxidative dissolution of the deposits of Cu and Ag formed as a result of the previous reduction of the respective corrosion products at more negative potentials. Neglecting

the contribution of the A_2 peak (in general clearly lower than the peak A_1), the peak current of A_1 , $i(A_1)$, can be approached by:

$$i(A_1) = \varepsilon_{\text{Cu}} n_{\text{Cu}} + \kappa \varepsilon_{\text{Ag}} n_{\text{Ag}} \quad (8)$$

Where n_{Cu} , n_{Ag} denote the number of Cu and Ag grains per volume unit electrochemically generated in the microparticulate deposit and κ is a numerical factor representative of the degree of overlapping between the stripping signals for the oxidative dissolution of Cu and Ag. Using the same approximation as above, one obtains:

$$i(A_1) = \frac{\varepsilon_{\text{Cu}} n_{\text{cup}}^{\circ} + \kappa \varepsilon_{\text{Ag}} n_{\text{AgCl}}^{\circ}}{\varepsilon_{\text{cup}} n_{\text{cup}}^{\circ} + \varepsilon_{\text{AgCl}} n_{\text{AgCl}}^{\circ}} i(C_1) - \frac{S^{-\beta} \kappa \varepsilon_{\text{Ag}} n_{\text{AgCl}}^{\text{sup}}}{(1 + \beta)(\varepsilon_{\text{cup}} n_{\text{cup}}^{\circ} + \varepsilon_{\text{AgCl}} n_{\text{AgCl}}^{\circ})^{1+\beta}} i(C_1)^{1+\beta} \quad (9)$$

This equation predicts a variation of $i(A_1)$ on $i(C_1)$ which, assuming that S remained approximately constant, can be expressed as:

$$i(A_1) = Mi(C_1) + Ni(C_1)^{\delta} \quad (10)$$

where the coefficients M and N depend on the composition of the corrosion products of copper and silver in the extremes of the secondary patina. Eq. (10), as Eq. (7), can be experimentally tested.

Another experimental test can be obtained on considering the current measured for the HER at a given potential, $i(\text{HER})$. Since, as occurring for lead [34], the reduction of H^+ (aq) at Cu- or Ag-plated graphite occurs much more easily than at the bare graphite surface, one can assume that the current for this process will depend on the surface area of graphite which is exposed to the electrolyte solution; i.e., that not covered by the solid sample, plus the contribution due to the catalytic effect of the metals deposited in the previous cathodic processes for the reduction of copper and silver corrosion products:

$$i(\text{HER}) = h_{\text{HER}} (S_o - S) + h_{\text{Cu}} n_{\text{Cu}} + h_{\text{Ag}} n_{\text{Ag}} \quad (11)$$

Here, S_o denotes the total electrode area and the h -coefficients are characteristic of each process and depend on the electrochemical conditions of operation (pH, scan rate, etc.). Taking into account the previous considerations, one can write:

$$i(\text{HER}) = h_{\text{HER}} (S_o - S) + S h_{\text{Cu}} n_{\text{cup}}^o z + \frac{S h_{\text{Ag}}}{1 + \beta} \left[(1 + \beta) n_{\text{AgCl}}^o z - n_{\text{AgCl}}^{\text{sup}} z^{1+\beta} \right] \quad (12)$$

Using the previous assumptions, one obtains:

$$i(\text{HER}) = h_{\text{HER}} (S_o - S) + \frac{h_{\text{Cu}} n_{\text{cup}}^o + h_{\text{Ag}} n_{\text{AgCl}}^o i(C_1)}{\varepsilon_{\text{cup}} n_{\text{cup}}^o + \varepsilon_{\text{AgCl}} n_{\text{AgCl}}^o} + \frac{S^{-\beta} n_{\text{AgCl}}^{\text{sup}} i(C_1)^{1+\beta}}{(1 + \beta) (\varepsilon_{\text{cup}} n_{\text{cup}}^o + \varepsilon_{\text{AgCl}} n_{\text{AgCl}}^o)^{1+\beta}} \quad (13)$$

Assuming, as before, that S remains practically constant, this equation predicts a variation of $i(\text{HER})$ on $i(C_1)$ of the form,

$$i(\text{HER}) = H + Gi(C_1) + Ri(C_1)^\delta \quad (14)$$

which can also be experimentally tested.

3.5. Characterization of monetary emissions

The model presented in the precedent section yields a satisfactory agreement with experimental data for the different sub-series of *maravedís*, as shown in Figure 4 where $i(C_2)/i(C_1)$ vs. $i(C_1)$ plots for *maravedís* minted in Madrid are overmarked. Experimental data for the different subseries of coins (*vide infra*) produced $i(C_2)/i(C_1)$ vs. $i(C_1)$ plots which were consistent with the theoretical expectances from Eq. (7). Pertinent statistical data for the fitting of experimental voltammetric parameters to Eq. (10) are summarized in Table 1. Apparently, the increase in the silver content determines a general increase of the $i(C_2)/i(C_1)$ ratio (see Figure 4). This feature can be interpreted on assuming that the $\varepsilon_{\text{AgCl}}$ parameter is lower than the ε_{cup} one, so that an increase of the AgCl contribution to peak C_1 results in a diminution of the peak current relative to that consisting of an equivalent contribution of cuprite alone.

Similar agreement between theoretical predictions and experimental data were obtained for the variation of $i(A_1)$ on $i(C_1)$ (Eq. (10), data in Figure 6) and $i(\text{HER})$ on $i(C_1)$ (Eq. (14), data in Figure 7). For our purposes, the relevant point to emphasize is that there are differences not only between the coins minted in different mints but also between coins produced in the same **mint** in successive years. This is illustrated in Figure 6 in which the variation of $i(A_1)$ on $i(C_1)$ for *maravedís* minted in Segovia (squares), Burgos (circles), Granada (triangles) and Seville (rhombs) in the period 1661-1664 is depicted. One can see in this figure that all 1661 coins (empty figures) can be grouped into a common tendency line agreeing with Eq. (10) whereas the coins minted between 1662 and 1664, although exhibiting more data dispersion, can be fitted to a clearly different tendency line also able to be described with this equation.

The variation of $i(\text{HER})$ on $i(C_1)$ is shown in Figure 7 for coins minted in Burgos, Segovia and Seville. In agreement with previous results, different sub-sets of data can be fitted to potential curves consistent with Eq. (14). All Segovia coins were grouped within the same tendency line whereas the coins minted in Burgos and Seville in 1661 were separated from those respectively manufactured in such mints in 1663.

The production of the Madrid mint is shown in Figure 8 in which the variation of the $i(C_2)/i(C_1)$ current ratio on $i(C_1)$ is depicted for *maravedís* in this study overmarking the coins minted in Segovia in 1661 and 1663 and Granada in 1662 and 1663 (triangles). Interestingly, the majority of the tested *maravedís* produced in the Madrid mint in 1661 (see Figure 4 and Table 1) displayed a pattern essentially identical to those of other mints in the same year. However, the coins fabricated in 1661 and 1662 were equivalent to those produced in other mints in the period 1662-1664.

The electrochemical grouping of the studied coins can be summarized (see statistical data for fitting of $i(C_2)/i(C_1)$ vs. $i(C_1)$ plots to Eq. (7) in Table 1) as:

a) Studied coins minted in 1661 in Burgos, Segovia and Seville and the majority of those **minted** in Madrid in 1661 were ascribed to the Madrid-I type.

b) The coins of the type Madrid-II were **minted** in this city in 1661 and 1662-1663, as well as in those from all other mints dated in 1662-1664 except coins from Segovia and Cuenca **(type I)**.

c) Madrid-III type coins were **minted** in Madrid in 1664 and Córdoba, 1664.

These features can be interpreted taking into account that, as a result of the existing inflationary pressure, incremented by the crisis of the agriculture and textile industry [59,60], the Spanish Treasury increased indirect taxes and since 1599 resorted to manipulating its low-value copper currency by means of the debasement of the Castilian *maravedí*, either through issues of petty copper coins, as in 1599–1606, 1617–19, 1621–6, and 1661–5, or through increases in its face value (*resellos*), as in 1603, 1634, 1636, 1641, 1643, 1651, 1653, and 1658 [40,45-47]. Both methods involved reducing (or even removing) the silver content of the *maravedí*, thus resulting in serious losses in the real wages of building laborers and craftsmen between 1621 and 1680 [46]. **In this context, the brief silver re-introduction between 1661 and 1664, was unable to contain the inflationary effects, so that** in 1680–1686 the Treasury implemented a deflationary program based on a realignment of the silver content of the Castilian petty coins and their face value. Our data can be summarized as:

a) In principle, coins minted in 1661 were produced by hammer. These are the Madrid-I type *maravedís*.

b) In 1661, the composition was altered upon lowering the silver content and/or the mint procedure was modified passing from hammer to mill. This occurred at least in the mints of Madrid, Burgos, Cuenca, Granada, Sevilla, Trujillo and Valladolid (Madrid-II type) and a second alteration was carried out in 1663 or 1664 (Madrid-III type) detected in the mints of Madrid, and Córdoba.

c) However, the Madrid-I norm, however, remained apparently unchanged until 1664 in the mint of Segovia.

d) Falsifications produced a clearly different voltammetric profile, the data points for the two coins **recognized as counterfeits** falling in a region of the diagrams clearly separated from the official currency (see Figure 8).

These data suggest that the 1661 norm was debased promptly, at least in several mints (including Madrid, that presumably produced an important fraction of all the currency), although remained operative in several mints. These features can be attributed to the replacement of the mint procedure from hammer to mill but also to the lowering of the silver content. In fact, as recently investigated by Andrés-Ucendo and Lanza-García [46], the currency manipulations between 1621 and 1680 produced serious losses in the real wages of building laborers and craftsmen. In particular, in the 1661-1665 years the real wages of both groups diminished significantly.

4. Conclusions

The voltammetric response of nanosamples from Spanish *maravedis* minted in the period 1661-1664 in the mints of A Coruña, Burgos, Córdoba, Cuenca, Granada, Madrid, Trujillo, Segovia, Seville and Valladolid was studied using the voltammetry of immobilized particles methodology. Characteristic voltammetric features of the main corrosion products, cuprite and AgCl, also identified by Raman spectroscopy, and those corresponding to the stripping peaks of Cu and Ag as well as the current for the hydrogen evolution reaction were used for screening the studied coins. A consistent grouping into three electrochemical types was obtained combining different pairs of voltammetric signals.

The obtained data suggested that the voltammetric signatures depended on the proportion of silver and the manufacturing procedure, thus resulting in significant differences characterizing the monetary emissions. Such electrochemical data: i) confirmed the existence of a hiatus in the production of currency as early as 1661 associated to a diminution in the silver content and/or change from hammer to mill fabrication; ii) however, the disruption was apparently non-uniformly followed by all mints and iii) possibly, the currency was further devaluated in several mints in 1664 by means of a drastic lowering of the silver content.

All these results illustrate the capability of voltammetric techniques to provide analytical information, acting as an archaeometric tool complementing the scope of available techniques.

Acknowledgements: Financial support from the MICIN Projects CTQ2014-53736-C3-1-P and CTQ2014-53736-C3-2-P, which are also supported with ERDF funds, is gratefully acknowledged. Thanks to the Museum of Prehistory of Valencia for facilitating the access to its collections.

References

- [1] D. A. Scott, *Metallography and Microstructure of Ancient and Historic Metals*, The Getty Conservation Institute, Paul Getty Museum, Malibu, 1991.
- [2] I. Constantinides, M. Gritsch, A. Adriaens, H. Hutter, F. Adams, *Anal. Chim. Acta* **2001**, *440*, 189.
- [3] R. Linke, M. Schreiner, *Mikrochim. Acta* **2000**, *133*, 165.
- [4] M. Dowsett, A. Adriaens, *Nucl. Inst. Meth. Phys. Res. B* **2004**, *226*, 38.
- [5] S. Shalev, S. Sh Shilstein, Yu Yekutieli, *Talanta* **2006**, *70*, 909.
- [6] R. Gaudiuso, M. Dell'Aglio, O. De Pascale, S. Loperfido, A. Mangone, A. De Giacomo, *Anal. Chim. Acta* **2014**, *813*, 15.
- [7] J. M. del Hoyo-Meléndez, P. Swit, M. Matosz, M. Wozniak, A. Klisinska-Topacz, L. Bratasz, *Nucl. Inst. Meth. Phys. Res. B* **2015**, *349*, 6.
- [8] M. Tomassetti, F. Marini, R. Bucci, L. Campanella, *Trends Anal. Chem.* **2016**, *79*, 371.
- [9] P. Budd, D. Gale, A. M. Pollard, R. G. Thomas, P. A. Williams, *Archaeometry* **1993**, *35*, 241.
- [10] D. Attanasio, G. Bultrini, G. M Ingo, *Archaeometry* **2001**, *43*, 529.
- [11] D. A. Scott, *J. Am. Ite. Cons.* **1994**, *33*, 1.
- [12] I. Constantinides, A. Adriaens, F. Adams, *Appl. Surf. Sci.* **2002**, *189*, 90.
- [13] L. Robbiola, R. Portier, *J. Cult. Herit.* **2006**, *7*, 1.
- [14] I. Sandu, C. Marutoiu, I. G. Sandu, A. Alexandru, A. V. Sandu, *Acta Universitatis Cibinensis Section F Chemia* **2006**, *9*, 39.
- [15] L. Robbiola, J. -M. Blengino, C. Fiaud, *Corr. Sci.* **1998**, *40*, 2083.
- [16] L. Robbiola, L. -P. Hurtel, Standard nature of the passive layers of buried archaeological bronze - The example of two Roman half-length portraits, in I. MacLeod, S. Pennec, L. Robbiola, Eds., *METAL 95*, James & James Science Publ., London, 1997, pp. 109–117.
- [17] F. Scholz, B. Meyer, Voltammetry of solid microparticles immobilized on electrode surfaces, *Electroanalytical Chemistry, A Series of Advances*, Bard, A. J., and Rubinstein, I., Eds., Marcel Dekker, New York, 1998, vol. 20, pp. 1–86.

- [18] F. Scholz, U. Schröder, R. Gulabowski, A. Doménech-Carbó, *Electrochemistry of Immobilized Particles and Droplets*, 2nd edit. Springer, Berlin-Heidelberg, 2014.
- [19] A. Doménech-Carbó, J. Labuda, F. Scholz, *Pure Appl. Chem.* **2013**, *85*, 609.
- [20] A. Doménech-Carbó, M. T. Doménech-Carbó, V. Costa, *Electrochemical Methods in Archaeometry, Conservation and Restoration*, Monographs in Electrochemistry Series, F. Scholz, Edit. Springer, Berlin-Heidelberg, 2009.
- [21] V. Costa, K. Leysens, A. Adriaens, N. Richard, F. Scholz, *J. Solid State Electrochem.* **2010**, *14*, 449.
- [22] F. Arjmand, A. Adriaens, *J. Solid State Electrochem.* **2012**, *16*, 535.
- [23] N. Souissi, L. Bousselmi, S. Khosrof, E. Triki, *Mater. Corros.* **2004**, *55*, 284.
- [24] M. Serghini-Idrissi, M. C. Bernard, F. Z. Harrif, S. Joiret, K. Rahmouni, A. Srhiri, H. Takenouti, V. Vivier, M. Ziani, *Electrochim. Acta* **2005**, *50*, 4699.
- [25] A. Doménech-Carbó, M. T. Doménech-Carbó, I. Martínez-Lázaro, *Microchim. Acta* **2008**, *162*, 351.
- [26] D. Satovic, S. Martinez, A. Bobrowski, *Talanta* **2010**, *81*, 1760.
- [27] A. Doménech-Carbó, M. T. Doménech-Carbó, J. Redondo-Marugán, L. Osete-Cortina, M. V. Vivancos-Ramón, *Electroanalysis* **2016**, *28*, 833.
- [28] D. Blum, W. Leyffer, R. Holze, *Electroanalysis* **1996**, *8*, 296.
- [29] A. Doménech-Carbó, M. T. Doménech-Carbó, M. A. Peiró-Ronda, *Electroanalysis* **2011**, *23*, 1391.
- [30] A. Doménech-Carbó, M. Lastras, F. Rodríguez, L. Osete-Cortina, *Microchem. J.* **2013**, *106*, 41.
- [31] A. Doménech-Carbó, M. T. Doménech-Carbó, I. Martínez-Lázaro, *Anal. Chim. Acta* **2010**, *610*, 1.
- [32] A. Doménech-Carbó, M. T. Doménech-Carbó, M. A. Peiró-Ronda, L. Osete-Cortina, *Archaeometry* **2011**, *53*, 1193.
- [33] A. Doménech-Carbó, M. T. Doménech-Carbó, M. Lastras, M. Herrero, *For. Sci. Int.* **2015**, *247*, 79.
- [34] A. Doménech-Carbó, M. T. Doménech-Carbó, M. A. Peiró-Ronda, *Anal. Chem.* **2011**, *83*, 5639.
- [35] A. Doménech-Carbó, M. T. Doménech-Carbó, S. Capelo, T. Pasíes-Oviedo, I. Martínez-Lázaro, *Angew. Chem. Int. Ed.* **2014**, *53*, 9262.

- [36] A. Doménech-Carbó, M. T. Doménech-Carbó, T. Pasíes-Oviedo, M.C. Bouzas, *Electroanalysis* **2012**, *24*, 1945.
- [37] A. Doménech-Carbó, J. Del Hoyo-Menéndez, M. T. Doménech-Carbó, J. Piquero-Cilla, *Microchem. J.* **2017**, *130*, 47.
- [38] F. Di Turo, N. Montoya, J. Piquero-Cilla, C. De Vito, F. Coletti, G. Favero, A. Doménech-Carbó, *Anal. Chim. Acta* **2017**, *955*, 36.
- [39] A. Doménech-Carbó, M. T. Doménech-Carbó, E. Montagna, Y. Lee, *Talanta* **2017**, *169*, 50.
- [40] P. Rueda Rodríguez-Vila, R. López Cortés, *Omni* **2012**, *5*, 96.
- [41] X. Sanahuja-Anguera, *Gaceta Numismática* **2012**, *184*, 15.
- [42] R. De Fontecha y Sánchez, *La moneda de vellón y cobre de la monarquía española (Años 1516 a 1931)*, Artes gráficas, Madrid, 1968.
- [43] A. Almenara, *Numisma* **2009**, *253*, 101.
- [44] R. C. Allen, *Econ. Hist. Rev.* **2003**, *LVI*, 403.
- [45] M. Drelichman, *Explor. Econ. Hist.* **2005**, *42*, 349.
- [46] J. I. Andrés-Ucendo, R. Lanza-García, *Econ. Hist. Rev.* **2014**, *67*, 607.
- [47] E. J. Hamilton, *War and prices in Spain, 1651–1800*, Cambridge, Mass., 1947.
- [48] A. Motomura, *Explor. Econ. Hist.* **1997**, *34*, 331.
- [49] L. Burgio, R. J. H. Clark, *Spectrochim. Acta A* **2001**, *57*, 1491.
- [50] Ł. Ciupiński, E. Fortuna-Zaleśna, H. Garbacz, A. Koss, K. J. Kurzydłowski, J. Marczak, J. Mróz, T. Onyszczuk, A. Rycyk, A. Sarzyński, W. Skrzeczanowski, M. Strzelec, A. Zatorska, G. Z. Żukowska, *Sensors* **2010**, *10*, 4926.
- [51] S. Capelo, P. M. Homem, J. Cavalheiro, I. T. E. Fonseca, *J. Solid State Electrochem.* **2013**, *17*, 223.
- [52] G. Cepriá, O. Abadías, J. Pérez-Arantegui, J. R. Castillo, *Electroanalysis* **2001**, *13*, 477.
- [53] D. Hamana, L. Boumaza, *J. Alloys Compd.* **2009**, *477*, 217.
- [54] M. B. McNiel, B. J. Little, *J. Am. Ite. Cons.* **1992**, *31*, 355.
- [55] R. J. H. Wanhill, *J. Fail. Anal. Prev.* **2011**, *11*, 175.
- [56] T. E. Graedel, *J. Electrochem. Soc.* **1992**, *139*, 1963.

[57] D. A. Scott, *Stud. Conservat.* **1997**, 42, 93.

[58] M. T. S. Nair, L. Guerrero, O. L. Arenas, P. K. Nair, *Appl. Surf. Sci.* **1999**, 150, 143.

[59] J.E. Gelabert, Urbanisation and deurbanisation in Castile, 1500–1800, in I.A.A. Thompson, B. Yun Casalilla, Eds., *The Castilian crisis of the seventeenth century: new perspectives on the economic and social history of seventeenth-century Spain*, Cambridge, 1994, pp. 182–206.

[60] R. Grafe, *Distant tyranny: markets, power, and backwardness in Spain, 1650–1800* Princeton, 2012.

Table 1. Statistical parameters for the fit to a potential law of $i(C_2)/i(C_1)$ vs. $i(C_1)$ curves for series of *maravedís* coins in this study. N corresponds to the number of data points taking into account that each coins was sampled in one, two or three different locations depending its conservation state.

Mint	Year of emission (number of coins)	N	A	α	r
Segovia	1661 (2), 1663 (2)	9	0.98 ± 0.02	$-(0.991\pm 0.018)$	0.9988
Granada	1662 (2), 1663 (2)	11	0.64 ± 0.10	$-(0.74\pm 0.09)$	0.938
Burgos	1661 (2) 1663 (1)	6	0.66 ± 0.06	$-(0.78\pm 0.06)$	0.987
Valladolid	1664 (2)	6	0.7 ± 0.3	$-(0.8\pm 0.2)$	0.84
Seville	1661 (3)	7	0.62 ± 0.12	$-(0.69\pm 0.11)$	0.938
Seville	1663 (1) 1664 (3)	8	0.7 ± 0.2	$-(0.8\pm 0.2)$	0.86
Madrid	1661 (6)	10	0.76 ± 0.05	$-(0.80\pm 0.05)$	0.984
Madrid	1662 (5) 1663 (2)	11	0.53 ± 0.07	$-(0.65\pm 0.07)$	0.957
Madrid	1664 (2)	6	0.44 ± 0.14	$-(0.62\pm 0.12)$	0.930
Trujillo	1664 (1)	3	0.60 ± 0.05	$-(0.63\pm 0.04)$	0.998
Cordoba	1664 (1)	3	0.59 ± 0.07	$-(0.83\pm 0.07)$	0.996
Cuenca	1664 (1)	3	0.48 ± 0.16	$-(0.63\pm 0.13)$	0.978

Figures

Figure 1. Raman spectrum and photographic image of coin M30 (• is cuprite Cu_2O bands and ♦ is tenorite CuO bands). (Inset: Photographic image of the obverse (left) and reverse (right) coin M30)

Figure 2. SEM/EDX microanalysis of coins a) M22 and b) M01 and the mapping for the corresponding areas c) M22 and d) M1.

Figure 3. Square wave voltammograms (two or three independent replicate experiments) of samples from coins a,b) M35, c,d) M31 and e,f) M26 attached to graphite electrodes immersed into air-saturated 0.25 M HAc/NaAc at pH 4.50. Potential scan initiated at a,c,e) +1.25 V in the negative direction; b,d,f) –1.05 V in the positive direction; potential step increment 4 mV; square wave amplitude 25 mV; frequency 5 Hz. Dotted lines represent the base lines for peak current measurements.

Figure 4. Variation of the $i(C_2)/i(C_1)$ current ratio on $i(C_1)$ for *maravedís* produced in the Madrid mint in 1661 (circles) in 1661 and 1662 (triangles) and 1662-1664 (squares) overmarked over the entire set of data for *maravedís* in this study. Two or three spots for each coin are depicted. Continuous lines correspond to the fit of such sub-series of data to a potential law. Error bars corresponded to deviations of 5% in the values of the represented quantities.

Figure 5. FESEM-FIB of coins a,b) M19 and c,d) M22. Secondary electron images (a,c) and elemental depth profiles (b,d) recorded in trenches of ca. 10 μm length and ca. 15 μm depth generated by FIB in the region of interest in the coins.

Figure 6. Variation of $i(A_1)$ on $i(C_1)$ for *maravedís* minted in Segovia (squares), Burgos (circles), Granada (triangles) and Seville (rhombs). Continuous lines correspond to the fit of such sub-series of data to a potential law such as in Eq. (10). Base line for current measurements was depicted in Figure 3.

Figure 7. Variation of $i(\text{HER})$ on $i(\text{C}_1)$ for *maravedís* minted in Burgos, Segovia and Seville. Continuous lines correspond to the fit of such sub-series of data to a potential law such as in Eq. (14). Criteria for current measurements was depicted in Figure 3.

Figure 8. Variation of the $i(\text{C}_2)/i(\text{C}_1)$ current ratio on $i(\text{C}_1)$ for *maravedís* in this study. Two or three spots for each coin are depicted. Data for *maravedís* minted in Segovia in 1661 and 1663 and Granada in 1662 and 1663 have been overmarked as well as for the two coins considered as falsifications. Continuous lines correspond to the fit of such sub-series of data to a potential law. Error bars corresponded to deviations of 5% in the values of the represented quantities. Base line for current measurements was depicted in Figure 3.

Figure 1.

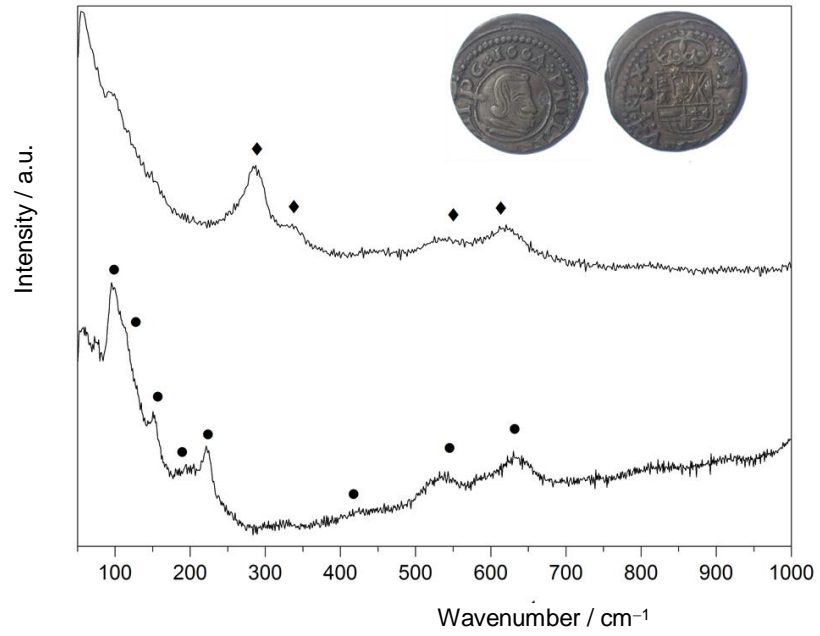


Figure 2.

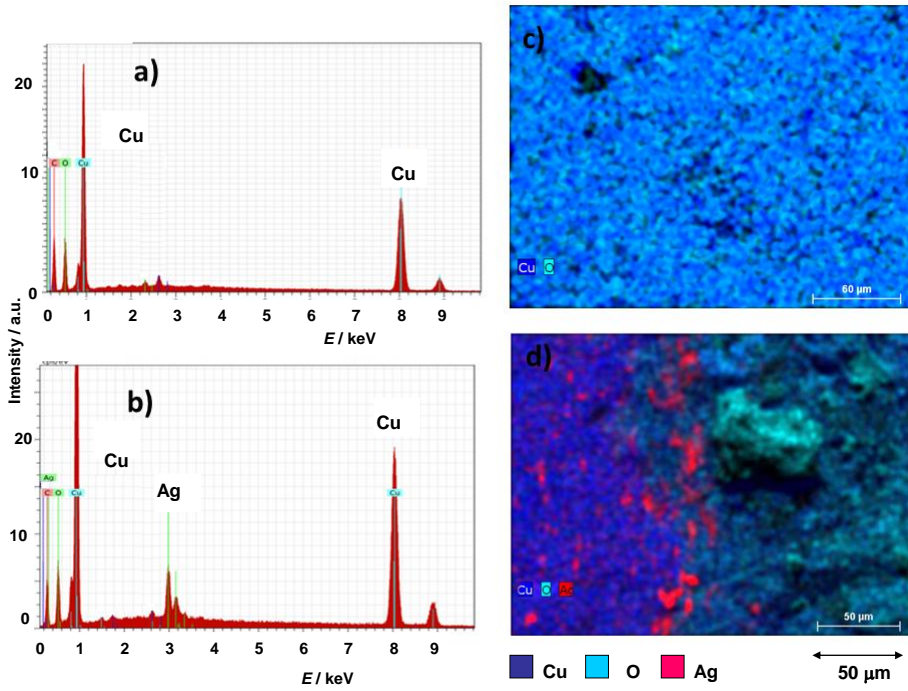


Figure 3.

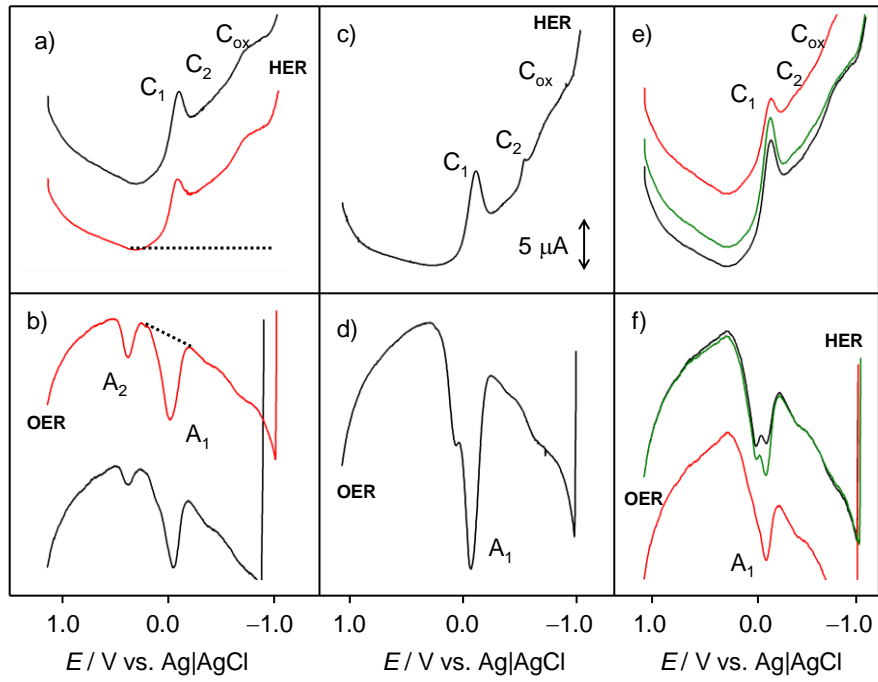


Figure 4.

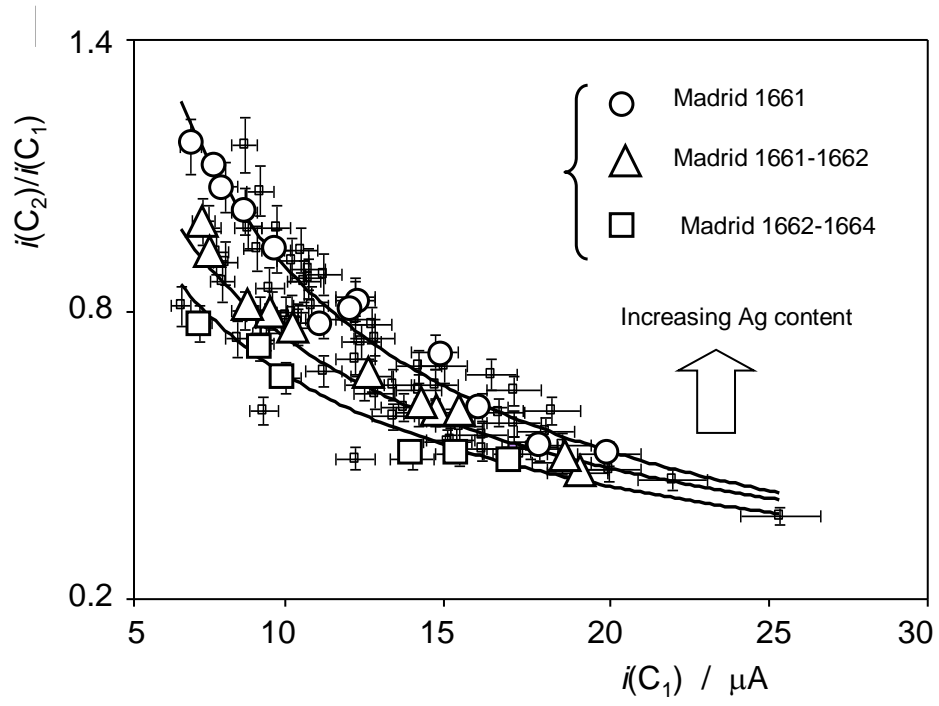


Figure 5.

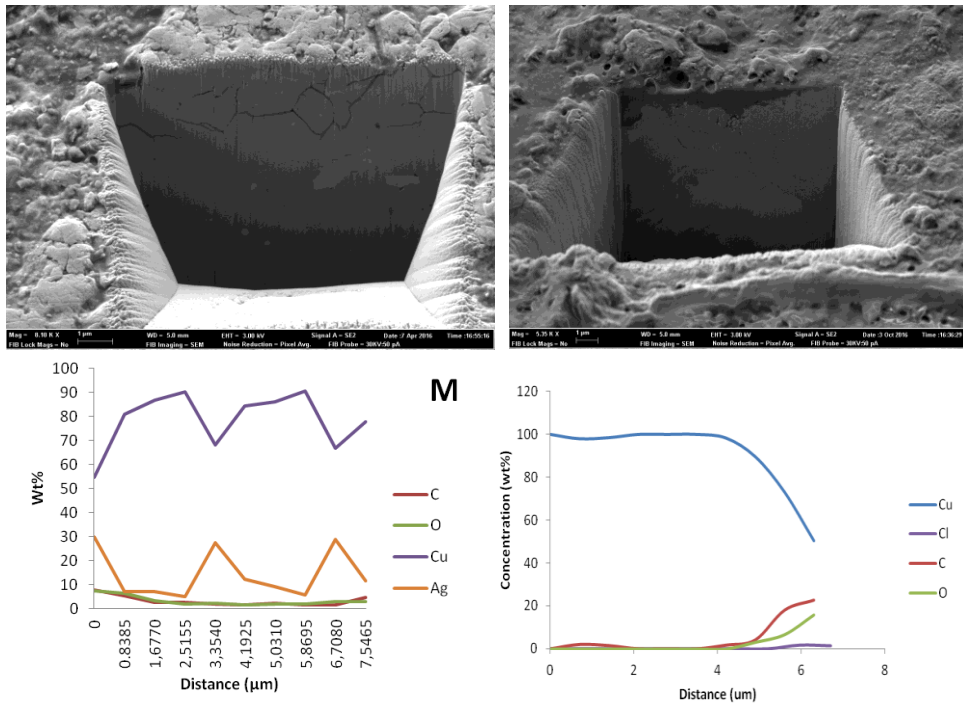


Figure 6.

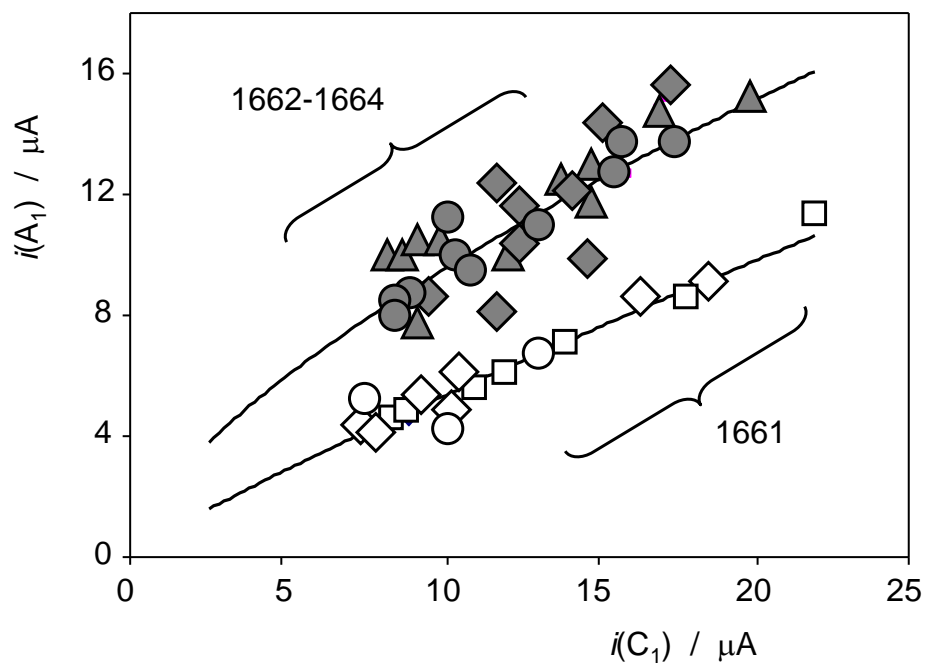


Figure 7.

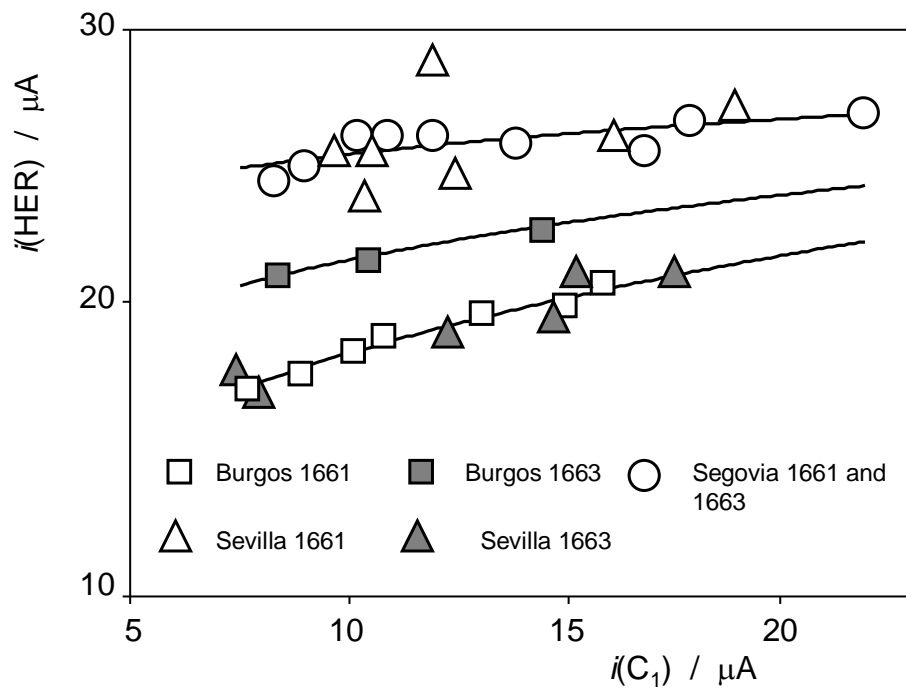


Figure 8.

